Journal of Materials Chemistry A

ROYAL SOCIETY OF CHEMISTRY

PAPER

View Article Online
View Journal

Cite this: DOI: 10.1039/d5ta05887b

A ductile and strong bioplastic film based on biodegradable polyurethane nanoparticle-crosslinked chitosan

Bo Chen, * Qiongyu Chen, Shuangshuang Jing, Taotao Meng and Teng Li *

The widespread use and disposal of petroleum-derived plastic films contribute significantly to environmental pollution, affecting water, soil, and air quality and leading to microplastic contamination. In response, extensive research has focused on developing biodegradable chitosan-based films with enhanced mechanical properties as alternatives to conventional plastics. However, balancing ductility and strength in chitosan-based materials remains a significant challenge because these two mechanical properties are intrinsically mutually exclusive. This study presents a facile strategy for fabricating chitosan/polyurethane nanoparticle (PU NP) bioplastic films that simultaneously enhance both ductility and strength. The chitosan/PU NP bioplastic film exhibits a unique and novel elastic node–grid structure, where PU NPs serve as crosslinkers (elastic nodes) within an entangled chitosan network. Notably, incorporating 20 wt% PU NPs results in a failure strain of 37.47%, a tensile strength of 64.98 MPa, and a tensile work to fracture of 17.50 MJ m^{-3}, representing increases of 311%, 23%, and 350%, respectively, compared with pure chitosan films. These remarkable mechanical properties are attributed to the deformation of the elastic nanoscale PU NPs under load and dynamic hydrogen bonding interactions between PU NPs and chitosan molecules. Furthermore, the bioplastic film is recyclable through a simple process without noticeable loss of mechanical performance and is compostable and biodegradable in soil within three months. This innovative bioplastic film holds promise for developing strong, ductile, and tough biopolymer materials, paving the way for sustainable alternatives to conventional plastic films and diverse future applications.

Received 21st July 2025
Accepted 4th November 2025

DOI: 10.1039/d5ta05887b

rsc.li/materials-a

Global plastic production has tripled over the past four decades, with projections indicating that greenhouse gas emissions from plastics could account for 15% of the global carbon budget by 2050.[1,2] This surge in petroleum-derived plastics has led to significant environmental issues, including pollution of oceans and rivers and the pervasive impact of microplastics on ecosystems.[3] In response, extensive efforts have focused on reducing plastic pollution and energy consumption by enhancing recyclability and developing eco-friendly alternatives, such as natural polymer-based packaging films for food and beverages,[4,5] biomass-based foams for atmospheric water harvesting,[6–8] and wood-based materials as substitutes for plastics.[9–11] Natural polymer-based films offer the advantages of renewability, sustainability, non-toxicity, and environmental friendliness. However, their mechanical properties often limit their direct replacement of commonly used plastics, such as polyethylene and polypropylene.[12,13] Thus, improving the ductility and strength of natural polymer-based films is essential.

Chitin, the second most abundant natural polymer on earth, is produced in vast quantities, approximately 100 billion tons annually, by fungi, plankton, the exoskeletons of insects, and crustaceans. Chitosan, derived from the deacetylation of chitin, contains amino and hydroxyl groups in its linear structure, facilitating hydrogen bond formation and resulting in water-solubility.[14–16] Due to their biodegradability and non-toxicity, chitosan films find widespread use in the food industry, bioelectronics, water treatment, and agriculture.[17–20] However, chitosan films exhibit poor ductility compared with conventional plastic films, primarily due to their higher oxygen and nitrogen content, which restricts the stretching and uncoiling of polymer molecules. Numerous strategies have been explored to enhance the ductility of chitosan films, including the incorporation of synthetic polymers, nanoclays, cellulose nanofibrils, metal oxides, and carbon nanotubes.[21–24] Yet, some of these approaches pose environmental risks, countering the ecological benefits of chitosan, while others lead to a trade-off between ductility and strength.[25,26] Consequently, developing a scalable technology for producing high-ductility and high-strength eco-friendly chitosan films remains a challenge.

Department of Mechanical Engineering, University of Maryland, College Park, Maryland 20742, USA. E-mail: bchen8@umd.edu; lit@umd.edu

Polyurethane (PU), a versatile family of thermoplastic elastomers, consists of hard and soft segments arranged in a linear structure.[27] Biodegradable PU can be synthesized using hydrolysis-prone polyester diols, such as poly(ε-caprolactone) (PCL) diol.[28] Notably, PCL diol-based PU exhibits hydrolysis rates approximately ten times faster than those of polyether diol-based PU, while the degradation products formed through hydrolysis demonstrate no significant cytotoxicity.[29,30] Incorporating biodegradable waterborne PU into chitosan-based materials has shown promise in enhancing mechanical properties.[31]

In this study, we report a facile yet effective method for fabricating chitosan/polyurethane nanoparticle (PU NP) bioplastic films that enhance both ductility and strength due to the novel node–grid structure formed by PU NPs as crosslinkers and the chitosan molecular network. By incorporating 20 wt% PU NPs, the bioplastic films achieve a failure strain of 37.47%, a tensile strength of 64.98 MPa, and a tensile work to fracture of 17.50 MJ m^{-3}, representing increases of 311%, 23%, and 350%, respectively, compared with pure chitosan films. These exceptional mechanical properties arise from the unique elastic deformation of nanoscale PU NPs under load and the dynamic hydrogen bonding interactions between PU NPs and chitosan molecules. Furthermore, the bioplastic films can be easily recycled without significant loss of mechanical performance and are biodegradable in soil within three months. This innovative bioplastic film is poised to serve as a valuable resource for developing strong, ductile, and tough biopolymer materials, offering potential alternatives to petroleum-derived plastic films and enabling various innovative future applications.

Results and discussion

Chitosan, a biodegradable polysaccharide obtained from shellfish shells, has numerous applications, including food packaging and antimicrobial materials (Fig. 1a). In this study, we developed a ductile, transparent, chitosan-based film using a simple cast-dry method, aiming for low-cost packaging solutions. Fig. 1 illustrates the fabrication process of the chitosan/PU NP bioplastic film, its mechanical performance, and the underlying deformation mechanism of the film to accommodate significant elongation.

The unique biodegradable waterborne PU NPs are synthesized *via* self-assembly in a water dispersion.[32–34] Scheme S1 shows the synthesis of the waterborne PU NPs. In brief, the PCL diol monomer and isophorone diisocyanate (IPDI) monomer serve as the soft and hard segments, respectively, for synthesizing the target PU polymeric chain. The resulting PU NPs adopt a core–shell structure (hydrophobic core and hydrophilic shell) upon the addition of ethylenediamine (EDA) and deionized water under vigorous mechanical stirring after prepolymerization. Fig. 1b and S1 depict the schematic representation and molecular formula of the core–shell structure, alongside the microstructure of the synthesized PU NPs.

To create the bioplastic film, the chitosan solution was mixed with varying amounts of PU NPs (0 wt%, 5 wt%, 10 wt%, 20 wt%, and 40 wt%, referred to as 0% PU, 5% PU, 10% PU, 20% PU, and 40% PU), and cast-dried in a fume hood at room temperature overnight. The PU NPs crosslink chitosan molecules *via* electrostatic interaction between the negatively charged carboxyl groups of PU NPs and the positively charged protonated amino groups of chitosan (protonated by acetic acid), along with multiple hydrogen bonds between PU NPs and chitosan. A representative transparent chitosan/PU NP bioplastic film (20% PU) is shown in Fig. 1c.

Mechanical testing reveals that the 10% PU and 20% PU bioplastic films exhibit significantly higher tensile strength, failure strain, and work to fracture in comparison with pure chitosan films (Fig. 1d). Specifically, the 20% PU films achieve a failure strain of 37.47 ± 1.66% and a tensile strength of 64.98 ± 3.20 MPa, which are approximately four times and 1.2 times greater than the failure strain (9.11 ± 1.86%) and strength (52.94 ± 4.74 MPa) of the 0% PU chitosan films. Additionally, the work to fracture for the 20% PU films is 17.50 ± 1.33 MJ m^{-3}, around 4.5 times higher than that of 0% PU chitosan films. This significant improvement in mechanical properties is attributed to the elastic node–grid structure formed by PU NPs serving as crosslinkers, with chitosan molecules entangled to create a robust network. The electrostatic interactions and hydrogen bonds facilitate the cross-linking between the PU NPs and chitosan molecules due to the abundant oxygen- and nitrogen-containing groups in chitosan and PU molecules, as shown in Fig. 1e and S2. Upon applying tensile force, the initially curly chitosan chains uncoil and disentangle, while the elastic PU NPs stretch from a spherical to an ellipsoidal shape to accommodate the tensile elongation.

Fig. S3a presents the Fourier-transform infrared (FTIR) spectra of PU NPs, 0% PU, 10% PU, and 20% PU, illustrating their distinct chemical compositions. The band between 3300 cm^{-1} and 3400 cm^{-1} corresponds to the characteristic absorption of O–H and N–H stretching vibrations in chitosan and water molecules.[6,7,9] The peaks at 2947 cm^{-1} and 2867 cm^{-1} are associated with the C–H_3 and C–H_2 stretching vibrations in the structures of PU and chitosan.[32] As shown in Fig. S3b, the absorption in the 1700–1750 cm^{-1} region for the chitosan film is ascribed to the carbonyl groups of the residual acetyl groups remaining after chitin deacetylation. The broad bands at 1556 cm^{-1} and 1537 cm^{-1} correspond to the N–H stretching and bending vibrations in PU and chitosan molecules, respectively. The unique peak at 1726 cm^{-1} is attributed to the vibration of C=O in the PU molecule. A small peak near 1726 cm^{-1} is observed when the PU content is increased to 20%, which is attributable to the presence of PU.

The scanning electron microscope (SEM) images in Fig. 2a and S4 reveal that the PU NPs, averaging around 500 nm in diameter, maintain a uniform spherical shape and are homogeneously dispersed within the chitosan matrix (Fig. 2b). As shown in Fig. S5, the distribution of PU NPs in water is mostly monodisperse (PDI = 0.3) with an intensity-weighted hydrodynamic diameter centered near 500 nm. The number-weighted distribution suggests a high frequency of occurrence of NPs sized around 300 nm. The size distribution of PU NPs in chitosan solution shows a similar pattern to that in water, indicating excellent dispersion stability of PU NPs. The mechanical

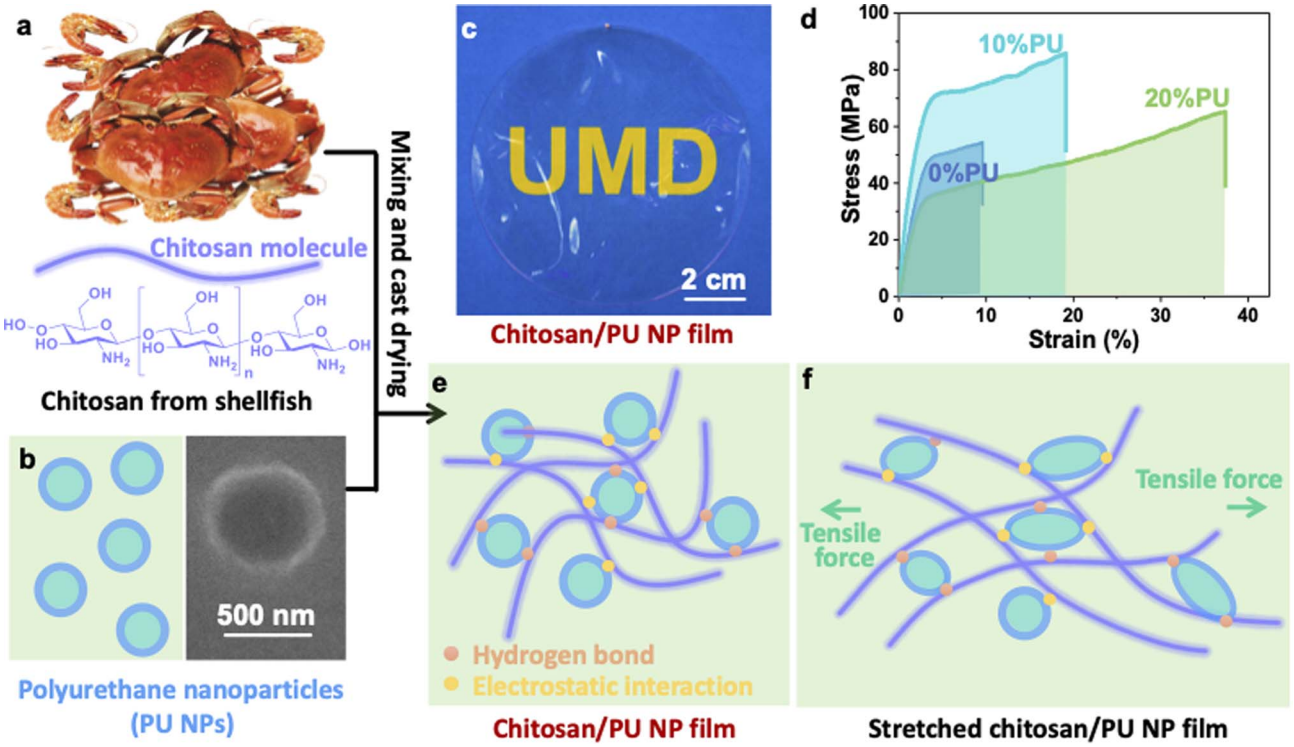

Fig. 1 Schematic of the facile fabrication of the chitosan/PU NP film and the mechanism of the elongation of chitosan/PU NP films. (a) Raw materials of chitosan. (b) Schematic and SEM image of the synthesized PU NPs. (c) As-fabricated transparent chitosan/PU NP film. (d) The stress–strain curves of various films with different concentrations of PU (*i.e.*, 0 wt%, 10 wt%, and 20 wt%). (e) Schematic representation for intermolecular hydrogen bonding interactions and electrostatic interactions between PU NPs and chitosan. (f) Schematic of the deformation of PU NPs in a stretched chitosan/PU NP film.

properties of the chitosan/PU NP bioplastic films, including tensile strain, tensile failure strength, and work to fracture, indicate a clear trend of improvement with increasing PU NP concentration (Fig. 2c–f and S6). The ductility (indicated by the tensile failure strain) of the bioplastic films (0% PU, 5% PU, 10% PU, 20% PU, and 40% PU) is 9.11 ± 1.86%, 13.28 ± 2.04%, 18.22 ± 2.21%, 37.47 ± 1.66%, and 40.01 ± 2.36%, respectively, demonstrating the excellent elasticity of PU NPs. While the failure strength increases initially with PU concentration, a decrease is observed at higher concentrations, possibly due to NP aggregation disrupting the molecular interaction both between and inside the polymer chains. The work to fracture also increases with PU concentration (*i.e.*, 3.89 ± 0.66 MJ m^{-3}, 6.23 ± 1.24 MJ m^{-3}, 11.56 ± 2.54 MJ m^{-3}, 17.50 ± 1.33 MJ m^{-3} and 16.33 ± 1.13 MJ m^{-3}), peaking at 17.50 ± 1.33 MJ m^{-3} for the 20% PU films. Table S1 lists the mechanical properties, processing methods, and sustainability metrics of various films made of chitosan, synthetic polymers, natural polymers, organic and inorganic nanoparticles. Compared with chitosan films reinforced with inorganic NPs, carbon nanotubes, natural polymer-derived NPs, and PEG, the chitosan/PU NP films in this work show superior tensile strength and ductility, as well as sustainability advantages.

Fig. 3a shows an optical image of a fractured film sample. Fig. 3b and c show SEM images of the fractured cross-section of the sample at different magnifications. The thickness of the fractured film is approximately 50–60 μm (Fig. 3b), demonstrating that the PU NPs are uniformly distributed throughout the composite film (Fig. 3c). Fig. 3d illustrates the significant elongation of the PU NPs, transforming from spherical to ellipsoidal shapes along the tensile load direction. Fig. 3c and d allow quantification of the aspect ratio of the stretched film. The as-prepared PU nanoparticles have an average diameter of ~500 nm. Upon stretching, their major and minor axes extend to approximately 1200 nm and 400 nm, respectively, giving an aspect ratio of approximately 3. This anisotropic deformation provides a mechanistic explanation for the excellent ductility observed in the composite film.

Based on these experimental results and analyses, we propose a mechanism for enhancing mechanical performance by forming an elastic node–grid structure in the chitosan/PU NP composite film, as illustrated in Fig. 3e–g. The PU NPs crosslink the chitosan molecules *via* electrostatic interactions between the negatively charged carboxyl groups on the PU NPs and the positively charged protonated amino groups on chitosan, in addition to multiple dynamic hydrogen bonds facilitated by the abundant oxygen- and nitrogen-containing groups in both chitosan and PU molecules.

The fracture mechanism occurs in three typical stages

Stage I: elastic deformation (0–3% strain, chitosan alignment). As the composite film is stretched, the coiled chitosan

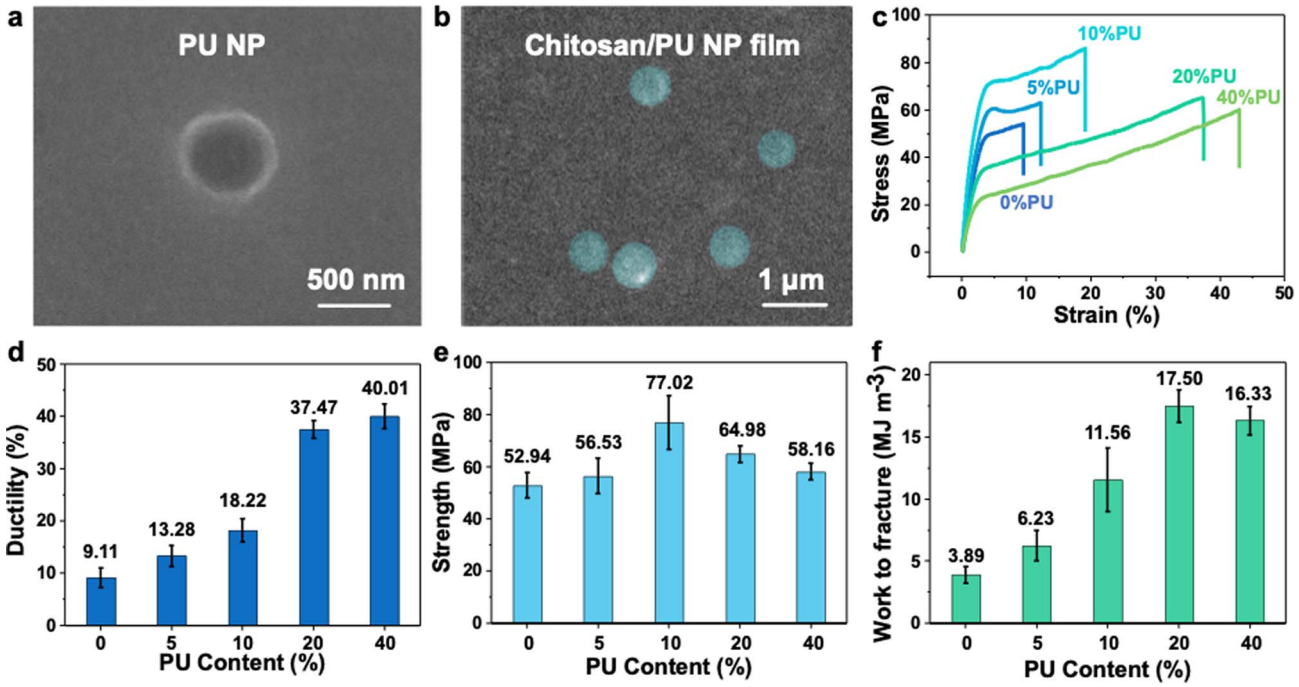

Fig. 2 Morphologies of PU NPs and mechanical properties of chitosan/PU NP composite films. (a) An SEM image of the as-fabricated PU NPs. (b) An SEM image of the as-fabricated chitosan/PU NP composite film showing that PU NPs are uniformly distributed in the chitosan film (*e.g.*, those highlighted in green). (c) The stress–strain curves of various films with different concentrations of PU (*i.e.*, 0 wt%, 5% wt%, 10 wt%, 20 wt%, and 40 wt%). (d–f) Comparison of the ductility (d), failure strength (e), and work to fracture (f) of the chitosan film and various composite films, respectively.

chains uncoil and disentangle. This process, occurring in the elastic deformation region (Fig. 3g), contributes to energy dissipation in the film. At this stage, the 10% PU sample exhibits higher stress than the 0% PU sample before yielding, likely due to the crosslinked nodes that hinder the disentanglement of the polymer chains. The chitosan polymer chains align along the tensile load direction. However, increasing PU NP content (20% and 40%) leads to a decrease in strength, which may be attributed to NP aggregation disrupting the molecular interaction both between and inside the polymer chains.

Stage II: yielding (strain beyond the elastic region, PU NP deformation). As stretching continues, the remarkable ductility of the PU NPs induces significant deformation in the yield region of the stress–strain curves. The 40% PU sample shows the largest strain before fracture. In this stage, the soft segments of the PU molecules entangle together to form the hydrophobic core of the PU NPs *via* van der Waals forces, while the repulsion between hydrophilic functional groups in the hard segments contributes to the overall molecular behavior. Under external tensile forces, the PU NPs elongate from spherical to ellipsoidal shapes. The van der Waals interactions between the soft segments of the PU NPs are overcome by the applied stress, leading to large deformation of the PU NPs, which plays a key role in energy dissipation during this phase. The electrostatic interaction and hydrogen bonds between PU NPs and chitosan chains are stronger than the van der Waals interaction in the soft segments of PU NPs, making the PU NPs act as elastic nodes to hold the chitosan grid structure and hinder sliding among chitosan chains which would otherwise result in the fracture of the film.

Stage III: fracture and crack propagation. Once the chitosan matrix and PU NP polymer chains reach their limit of stretch, further deformation is constrained. At this point, defects within the chitosan matrix initiate microcracks due to the fracture of hydrogen bonds. Some of the PU NPs recover their spherical shapes due to the brokerage of the hydrogen bonds between PU NPs and chitosan chains. The chitosan chains slide along the tensile load direction and separate from each other and from PU NPs, leading to the fracture of the whole elastic node–grid structure. These microcracks rapidly propagate into macrocracks, eventually leading to the failure of the entire composite film. The fracture of dynamic hydrogen bonds is the primary mechanism for energy dissipation during this final stage.

The thermal stability and optical properties of chitosan, PU, and chitosan/PU NP films were studied by TGA and UV-vis transmission analysis. The TGA curves of chitosan, PU, and chitosan/PU NP films are shown in Fig. S7. The typical decomposition pattern below 180 °C in chitosan and chitosan/PU NP films is ascribed to water evaporation. The degradation of chitosan and PU begins at 250 °C and 210 °C, respectively. Upon PU incorporation, the initial deposition temperature decreases to 175 °C. Chitosan films exhibit higher thermal stability at temperatures above 400 °C compared to pure PU films. The differential thermogravimetry (DTG) pattern of chitosan/PU NP films shows no new peaks, suggesting a uniform dispersion of

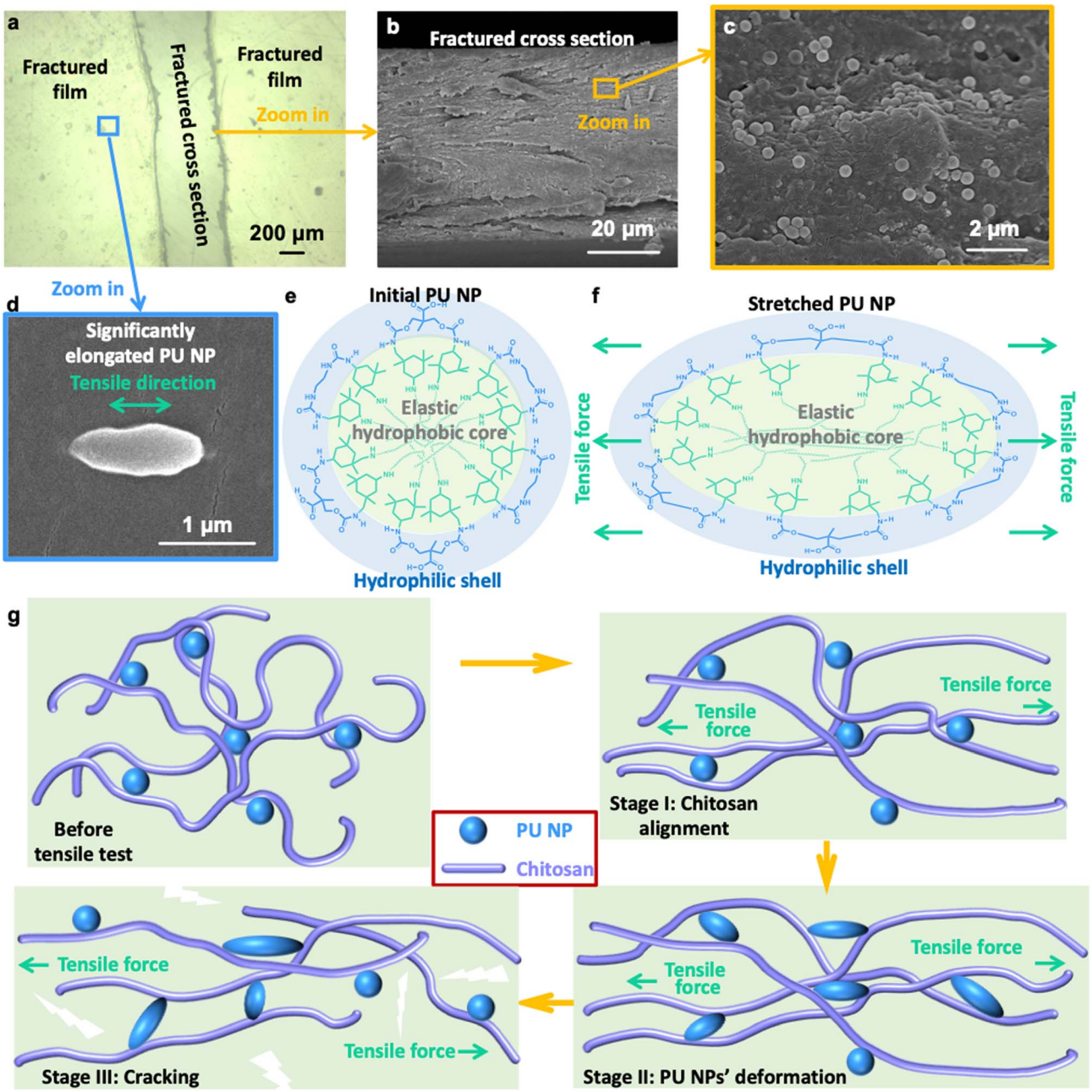

Fig. 3 The toughening mechanism of the elastic node–grid structure in chitosan/PU NP composite films. (a) An optical image of a fractured film sample. (b and c) SEM images of the cross-section of the composite film at different magnifications. (d) SEM image of a significantly elongated PU NP in the composite film under tensile force. (e) Schematic of the PU NP molecular core–shell structure. (f) Schematic of the molecular scale deformation of the PU NP under tensile force. (g) Schematic of the failure mechanism of the chitosan/PU NP film.

PU in the chitosan matrix. The UV-vis transmission spectra of chitosan and chitosan/PU NP films are shown in Fig. S8. With PU incorporation, UV light (under 400 nm) transmittance can be reduced from 60% to 1–35%. The chitosan/PU NP film exhibits impressive recyclability, contributing to reduced manufacturing costs and environmental sustainability. Fig. 4a outlines the recycling process for the composite film. After use, the film can be dispersed into water and reformed into a homogenous dispersion of PU NPs and chitosan by mechanical stirring for 1 hour. In this process, the electrostatic interaction and hydrogen bonds between the PU NPs and chitosan are disrupted, leading to the uncrosslinking of the chitosan molecules. Water molecules surround and interact with both the PU NPs and chitosan, facilitating their dispersion through electrostatic interactions and hydrogen bonding. The resulting dispersion can then be used to fabricate new chitosan/PU NP films, making the material fully recyclable. After recycling, the composite film retains its mechanical properties as shown in Fig. 4b–d. The ductility, tensile strength, and work to fracture of the recycled composite film are 31.56 ± 0.83%, 68.57

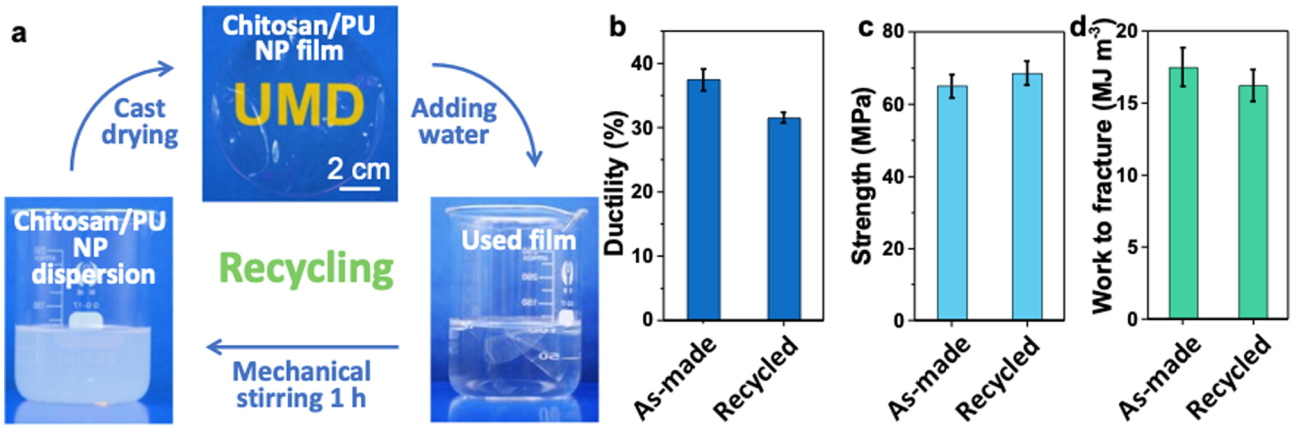

Fig. 4 Recyclability tests and mechanical properties of the recycled chitosan/PU NP film. (a) The recycling process of the as-made chitosan/PU NP film, including cast drying, water soaking, and mechanical stirring. (b–d) The comparison of the mechanical properties of the as-made and recycled composite films in terms of ductility (b), tensile strength (c), and work to fracture (d).

$\pm$ 3.36 MPa, and 16.23 $\pm$ 1.13 MJ m^{-3}, respectively, comparable to those of the as-made chitosan/PU NP film. This recyclability not only reduces material and manufacturing costs, but also minimizes resource waste.

The PU NPs are synthesized using a solvent-free and residue-free method. The waterborne PU, composed of PCL diol and IPDI, has been proven to have low cytotoxicity and excellent biodegradability in previous studies.[31,35] To evaluate the biodegradability and ecotoxicity of the chitosan/PU NP film, a grass seed germination test was conducted. Grass seeds were planted on the top surface of the soil at a density of approximately 12 pounds per 1000 square feet. The pure chitosan and 20% PU composite films were vertically buried in the soil in contact with the inner surface of a glass tank, as shown in Fig. 5 and S9. The test lasted for approximately two months. Most grass seeds began germinating within 10 days and continued growing throughout the experiment. The films were observed under both natural light (Fig. 5a and S9a) and UV 365 nm light (Fig. 5b, c and S9b) to monitor biodegradation. Under UV light, mold appeared on the films by Day 10 and increased progressively

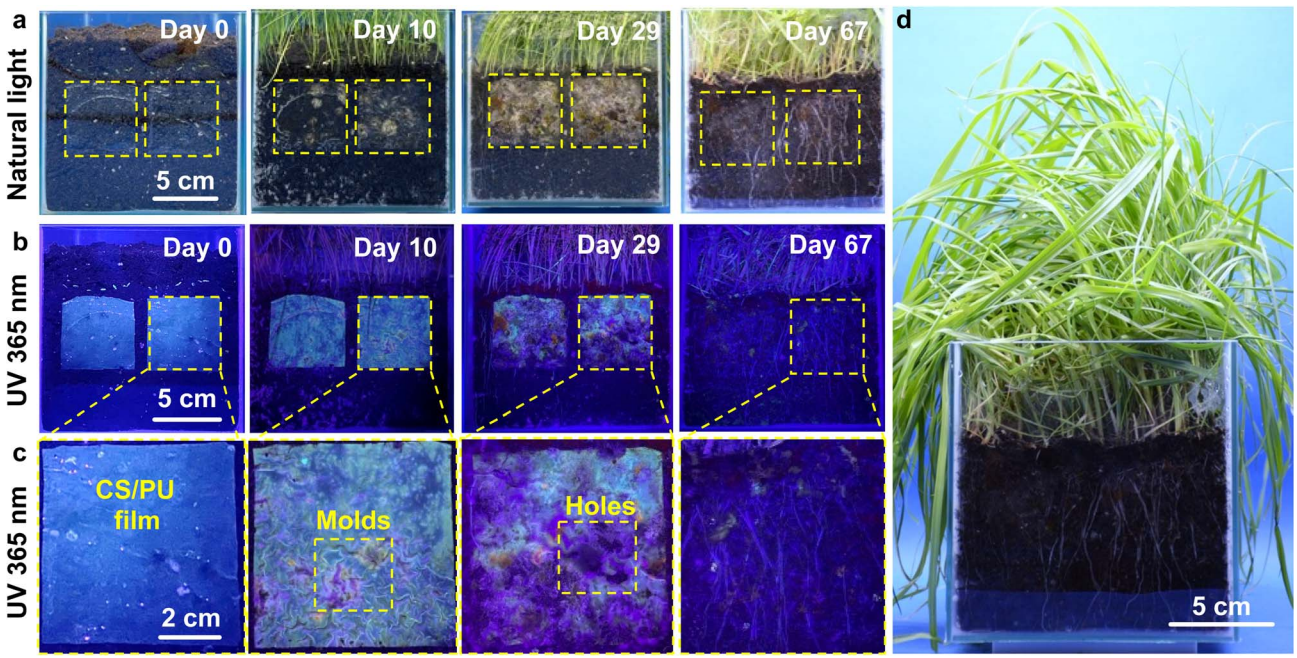

Fig. 5 Grass seed germination and plant growth tests to evaluate the biodegradability and ecotoxicity of the chitosan/PU NP composite film. In each test set, two pieces of the film (5 $\times$ 5 cm^2) are buried in soil together with some grass seeds in proximity. (a–c) The optical photographs of the film and the grass at different time intervals (*i.e.*, 0 to 67 days) under natural light (a) and UV 365 nm light (b and c). Mold is observed on Day 10, and holes begin to appear in the film after one month. By Day 67, the composite film is nearly completely degraded under both natural light and UV 365 nm light. (d) Snapshots of the test set show the successful germination and growth of the grass plant after two months.

throughout the test. By the end of the first month, holes were visible in the films, and by the end of the second month, the films had nearly completely biodegraded, as evidenced by their near-total disappearance under both natural light and UV 365 nm light (Fig. 5b, c, and S9b). Fig. 5d shows the grass plants after two months, with height ranging from 15–25 cm. The above ecotoxicity test and the control experiments demonstrate that the chitosan/PU NP film does not have any significant negative impact on seed germination or plant growth, suggesting that it is eco-friendly and biodegradable.

Conclusions

In conclusion, we present a cost-effective, straightforward method for producing biodegradable chitosan/PU NP composite films that enhance both the ductility and strength of chitosan-based materials. The chitosan/PU NP composite film exhibits an elastic node–grid structure at the microscopic level, where PU NPs act as crosslinking nodes and chitosan molecules form a grid-like structure. Incorporating 20 wt% PU NPs into the composite film results in significant improvements in mechanical properties, including a failure strain of 37.47%, a tensile strength of 64.98 MPa, and a work to fracture of 17.50 MJ m^{-3}. These values represent increases of 311%, 23%, and 350%, respectively, compared to pure chitosan films. These enhanced mechanical properties are attributed to the elastic deformation of the nanoscale PU NPs under load and the dynamic hydrogen bonding interactions between the PU NPs and chitosan molecules. Furthermore, the composite film demonstrates excellent recyclability, retains its mechanical performance after recycling, and biodegrades in soil within three months. The combination of biodegradability, recyclability, and enhanced mechanical properties make this composite film a promising candidate to replace conventional plastic films in a wide range of applications, contributing to sustainability and environmental protection.

Materials and methods

Synthesis of PU NPs

Waterborne PU NPs are synthesized using a waterborne procedure. Polycaprolactone diol (PCL, 10 g, $M_n \sim 2000$, ACROS ORGANICS, USA), which serves as the soft segment of the PU polymeric chain is first added into a 500 mL 3-neck flask under an Ar atmosphere and mechanically stirred for 30 min in a 75 °C water bath. Then, isophorone diisocyanate (IPDI, 4.18 g, 98%, ACROS ORGANICS, USA), which acts as the hard segment of the polyurethane chain, is introduced to the flask, and the prepolymerization is carried out for 3 h at 75 °C. Next, 2,2-bis(hydroxymethyl)propionic acid (DMPA, 0.699 g, Alfa Aesar, USA) as a chain extender together with methyl ethyl ketone (MEK, 0.038 g MACRON Fine Chemicals) is added into the flask and reacted for 1 h at 75 °C. After cooling the reaction mixture to 45 °C, triethylamine (TEA, 0.505 g, Fisher BioReagents, USA) is added dropwise into the flask to neutralize the carboxyl groups in DMPA for 30 min. Then, 36 mL of deionized water is rapidly added into the flask under vigorous stirring (1200 rpm) for 2 min, forming a milky mixture. Finally, ethylenediamine (EDA, 0.457 g, 99+%, ACROS ORGANICS, USA) as another chain extender diluted with deionized water is added and reacted for another 30 min. The residual MEK and TEA are removed by vacuum distillation. The molar ratio of IPDI/PCL/DMPA/TEA/EDA is 1/0.265/0.265/0.265/0.404 for the preparation of the PU NPs.

Fabrication of the chitosan/PU NP film

To prepare the chitosan/PU NP composite film, 50 mL 2 wt% acetic acid (Fisher Chemical, USA) solution is first prepared. Next, 0.25 g chitosan (medium molecular weight, Sigma-Aldrich, USA) powder is slowly added into the acetic acid solution under magnetic stirring to make 0.5 wt% chitosan solution. A predetermined amount of the PU dispersion is dropped into the chitosan solution to make chitosan/PU dispersion. Five different formulations are used to prepare the composite films with varying concentrations of PU NPs, *i.e.*, 0 wt%, 5 wt%, 10 wt%, 20 wt%, and 40 wt% (based on the mass of chitosan) which are denoted as 0% PU, 5% PU, 10% PU, 20% PU, and 40% PU in this paper. Then half of the resulting dispersion is poured into a Petri dish with a diameter of 90 mm. The dish is then covered with an air-permeable tissue and placed in a fume hood at room temperature overnight to form the chitosan/PU NP composite film. The next day, the film is carefully peeled from the Petri dish and cut into strips for the tensile test. The dimensions of the composite strips are approximately 60 mm by 5 mm by 50 μm. The films and strips are stored in a sealed bag for further use.

Characterization

The morphologies of the PU NPs and composite film samples were characterized using a Tescan XEIA3 SEM. Prior to SEM imaging, the samples were coated with a thin layer of gold *via* sputtering. A spectrometer (Thermo Nicolet NEXUS 670 FTIR, USA) with 4 cm^{-1} resolution was employed to obtain the FTIR spectra at room temperature. Tensile tests of the composite films were conducted using an Instron 5940 Series Single Column Table Frame equipped with a 1000 N load cell at a nominal displacement rate of 10 mm min^{-1}. The optical images of the microstructure of the films were taken using an optical microscope (ZEISS, Primo Star). DLS measurements were carried out on a ZETASIZER Nano-ZS (Malvern, UK). Transmittance spectra were measured using a UV-2600i UV-Vis spectrophotometer (Shimadzu, Japan). TGA was performed using an SDT Q600 (TA Instruments, USA) under a nitrogen atmosphere at a heating rate of 10 °C min^{-1}.

Conflicts of interest

There are no conflicts to declare.

Data availability

The data supporting this article have been included as part of the supplementary information (SI). Supplementary information is available. See DOI: **https://doi.org/10.1039/d5ta05887b**.

Acknowledgements

The support from the U.S. National Science Foundation (Awards #1936452 and # 2413847) and the University of Maryland Grand Challenges Grant is appreciated.

References

1 J. Zheng and S. Suh, *Nat. Clim. Change*, 2019, **9**, 374–378.
2 R. Geyer, J. R. Jambeck and K. L. Law, *Sci. Adv.*, 2017, **3**, e1700782.
3 A. Pellis, J. W. Comerford, S. Weinberger, G. M. Guebitz, J. H. Clark and T. J. Farmer, *Nat. Commun.*, 2019, **10**, 1–9.
4 M. Farooq, T. Zou, G. Riviere, M. H. Sipponen and M. Osterberg, *Biomacromolecules*, 2018, **20**, 693–704.
5 X. Zhao, Y. Wang, X. Chen, X. Yu, W. Li, S. Zhang, X. Meng, Z.-M. Zhao, T. Dong and A. Anderson, *Matter*, 2023, **6**, 97–127.
6 B. Chen, S. Jing, Q. Chen, Y. Pei, T. Deng, B. Yang, C. Wang and T. Li, *Nano Energy*, 2023, **110**, 108371.
7 B. Chen, X. Zhao and Y. Yang, *ACS Appl. Mater. Interfaces*, 2019, **11**, 15616–15622.
8 H. Xue, B. Chen and Y. Wang, *Langmuir*, 2024, **40**, 12810–12817.
9 B. Chen, U. H. Leiste, W. L. Fourney, Y. Liu, Q. Chen and T. Li, *Matter*, 2021, **4**, 3941–3952.
10 Y. Li, C. Chen, J. Song, C. Yang, Y. Kuang, A. Vellore, E. Hitz, M. Zhu, F. Jiang and Y. Yao, *Chin. J. Chem.*, 2020, **38**, 823–829.
11 B. Chen, Q. Chen, U. H. Leiste, Y. Liu, T. Meng, J. Dai, A. Gong, L. Hu, W. L. Fourney and T. Li, *Extreme Mech. Lett.*, 2024, **71**, 102218.
12 M. Peplow, *Nature*, 2016, **536**, 266–268.
13 X. F. Pan, B. Wu, H. L. Gao, S. M. Chen, Y. Zhu, L. Zhou, H. Wu and S. H. Yu, *Adv. Mater.*, 2022, **34**, 2105299.
14 T. Xu, H. Gao, J. Zhou, M. He, X. Ji, H. Dai and O. J. Rojas, *Int. J. Biol. Macromol.*, 2023, **229**, 321–328.
15 F. Ahmadijokani, H. Molavi, A. Bahi, S. Wuttke, M. Kamkar, O. J. Rojas, F. Ko and M. Arjmand, *Chem. Eng. J.*, 2023, **457**, 141176.
16 Z. Q. Fang, G. Chen, Y. S. Liu and X. S. Chai, *Appl. Mech. Mater.*, 2012, **200**, 180–185.
17 R. Priyadarshi and J.-W. Rhim, *Innovative Food Sci. Emerging Technol.*, 2020, **62**, 102346.
18 S. Aththanayaka, G. Thiripuranathar and S. Ekanayake, *Mater. Today Sustainability*, 2022, **20**, 100206.
19 E. Kim, Y. Liu, X. W. Shi, X. Yang, W. E. Bentley and G. F. Payne, *Adv. Funct. Mater.*, 2010, **20**, 2683–2694.
20 J. Sun, H. Choi, S. Cha, D. Ahn, M. Choi, S. Park, Y. Cho, J. Lee, T. e. Park and J. J. Park, *Adv. Funct. Mater.*, 2022, **32**, 2109139.
21 P. Song, Z. Xu, M. S. Dargusch, Z. G. Chen, H. Wang and Q. Guo, *Adv. Mater.*, 2017, **29**, 1704661.
22 B. Vollick, P.-Y. Kuo, H. Therien-Aubin, N. Yan and E. Kumacheva, *Chem. Mater.*, 2017, **29**, 789–795.
23 L. Liu, M. Zhu, X. Xu, X. Li, Z. Ma, Z. Jiang, A. Pich, H. Wang and P. Song, *Adv. Mater.*, 2021, **33**, 2105829.
24 P. Song, J. Dai, G. Chen, Y. Yu, Z. Fang, W. Lei, S. Fu, H. Wang and Z.-G. Chen, *ACS Nano*, 2018, **12**, 9266–9278.
25 Q. Zhang, Y. Chen, P. Wei, Y. Zhong, C. Chen and J. Cai, *Mater. Today*, 2021, **51**, 27–38.
26 M. I. Wahba, *J. Biomater. Sci., Polym. Ed.*, 2020, **31**, 350–375.
27 S.-h. Hsu, K.-C. Hung, Y.-Y. Lin, C.-H. Su, H.-Y. Yeh, U.-S. Jeng, C.-Y. Lu, S. A. Dai, W.-E. Fu and J.-C. Lin, *J. Mater. Chem. B*, 2014, **2**, 5083–5092.
28 F. Khan, S. Valere, S. Fuhrmann, V. Arrighi and M. Bradley, *J. Mater. Chem. B*, 2013, **1**, 2590–2600.
29 R. S. Labow, D. J. Erfle and J. P. Santerre, *Biomaterials*, 1996, **17**, 2381–2388.
30 L. Tatai, T. G. Moore, R. Adhikari, F. Malherbe, R. Jayasekara, I. Griffiths and P. A. Gunatillake, *Biomaterials*, 2007, **28**, 5407–5417.
31 T. W. Lin and S. h. Hsu, *Adv. Sci.*, 2020, **7**, 1901388.
32 Y.-P. Chen and S.-h. Hsu, *J. Mater. Chem. B*, 2014, **2**, 3391–3401.
33 Y.-J. Huang, K.-C. Hung, H.-S. Hung and S.-h. Hsu, *ACS Appl. Mater. Interfaces*, 2018, **10**, 19436–19448.
34 C.-W. Ou, C.-H. Su, U.-S. Jeng and S.-h. Hsu, *ACS Appl. Mater. Interfaces*, 2014, **6**, 5685–5694.
35 M. Indumathi and G. Rajarajeswari, *Int. J. Biol. Macromol.*, 2019, **124**, 163–174.

